Block Soft Decision Feedback Turbo Equalization for Orthogonal Signal-Division Multiplexing Underwater Acoustic Communications

Xiangzhao Qin[1,2], Fengzhong Qu[1], and Y. Rosa Zheng[2]

[1] – Key Laboratory of Ocean Observation-Imaging Testbed of Zhejiang Province,
Zhejiang University, Zhoushan, Zhejiang 316021, China.
[2] – Dept. of ECE, Lehigh University, Bethlehem, PA 18015-3084, USA.

Abstract—Orthogonal signal-division multiplexing (OSDM) is one of the generalized modulation schemes that bring the gap between orthogonal frequency division multiplexing (OFDM) and single carrier frequency domain equalization (SC-FDE). By performing encoding upon subvectors of each interleaved block, it enjoys a flexible resource management with low peak-to-average power ratio (PAPR). Meanwhile, the OSDM induces the intervector interference (IVI) inherently, which requires a more powerful equalizer. By deriving the input and output system model, this paper proposes a time domain soft decision feedback equalizer (SDFE) on per vector equalization with successful soft interference cancellation (SSIC). In addition, this paper takes the whole OSDM block to perform the channel encoding rather than on each vector of the OSDM. Simulation and experimental results demonstrate that the proposed SDFE with SSIC structure outperforms the conventional minimum mean square error (MMSE) equalizer and the block encoding (BE) scheme outperforms the vector encoding (VE) scheme, because theoretically the longer the encoded bit stream is, the more stable and more confident the maximum *a posteriori* probability (MAP) decoder will be.

Key words: Orthogonal signal-division multiplexing (OSDM), soft decision feedback equalizer (SDFE), successful soft interference cancellation (SSIC), block encoding (BE), Turbo equalization (TEQ), underwater acoustic (UWA) communications.

I. INTRODUCTION

Underwater acoustic (UWA) communication systems encounter significant technical challenges due to the doubly-selective fading channels that experience long delay spread and fast time-variation, coupled with the limited bandwidth. To achieve a reliable transmission with high bandwidth efficiency, both single carrier modulation (SCM) [1], [2] and orthogonal frequency division multiplexing (OFDM) communication systems [3], [4] have been comprehensively investigated over the past ten years. In the SCM scheme, the powerful Turbo receiver design has been widely adopted to combat the severe intersymbol interference (ISI) and Doppler effect, but its time domain equalizer (TDE) requires high computational complexity and its the frequency domain equalizer (FDE) suffers inflexible bandwidth and energy management. Compared to the SCM, the OFDM enjoys the reduced computational complexity via IFFT and FFT processing, but suffers from the low bandwidth efficiency and high peak-to-average power ratio (PAPR). Moreover, the approximated one tap equalizer design is insufficient for OFDM due to the severe frequency selectivity in UWA channels. Therefore, new physical layer scheme such as waveform design is desired to have robust performance, moderate receiver complexity, flexible bandwidth management while keeping fine energy tuning.

The newly emerging 5G waveform candidates such as filter-bank multicarrier (FBMC) [5], generalized frequency division multiplexing (GFDM) [6], and non-orthogonal multiple access (NOMA) [7] are potentially selected as the physical layer scheme for UWA communications. However, these approaches require explicit interference cancellation (IC) which needs an elaborate derivation of the equivalent system model. Moreover, there's no significant evidence to demonstrate that these non-orthogonal approaches perform better than the conventional OFDM in UWA communications.

The orthogonal signal-division multiplexing (OSDM) scheme is a promising approach to address the drawbacks above inherent to the OFDM scheme and the corresponding non-orthogonal multicarrier schemes, preserving the advantages of the flexible bandwidth and energy management. Also, the OSDM that originates from [8], [9] has been evaluated in UWA communications [10]–[13]. Different from [12], [13] that design an approximated frequency domain (FD) MMSE equalizer, this paper proposes a time domain (TD) per vector soft decision feedback equalizer (SDFE) by deriving the equivalent system model for turbo OSDM scheme. Simulation results demonstrate that the time domain SDFE outperforms the time domain MMSE equalizer and the per block encoding (BE) scheme has better BER performance than the per vector encoding (VE) scheme. The similar conclusion is also drawn from the experimental results.

II. SYSTEM MODEL

Consider a bit-interleaved coded modulation (BICM) UWA system with $\mathbf{c} = [\mathbf{c}_0^T, \ldots, \mathbf{c}_n^T, \ldots, \mathbf{c}_{N-1}^T]^T$ being the interleaved encoded bit vector. For the vector encoding (VE) scheme in [12], [13], substreams $\mathbf{c}_n = [\mathbf{c}_{n,0}^T, \ldots, \mathbf{c}_{n,m}^T, \ldots, \mathbf{c}_{n,M-1}^T]^T$ are generated by N different interleavers in parallel, then the corresponding code word

vector $\mathbf{c}_{n,m}^T = [c_{n,m}^1, c_{n,m}^2, \ldots, c_{n,m}^q]^T$ is mapped onto a given constellation in set $\mathcal{S} = [\alpha_1, \alpha_2, \ldots, \alpha_{2^q}]^T$, formatting a baseband symbol vector $\mathbf{x} = [\mathbf{x}_0^T, \mathbf{x}_1^T, \ldots, \mathbf{x}_{N-1}^T]^T$ with the block length being $K = NM$, where $\mathbf{x}_n = [x_{n,0}, x_{n,1}, \ldots, x_{n,M-1}]^T$. Instead of using N independent interleavers, the block encoding (BE) scheme adopts one interleaver to generate $\mathbf{c}$, then leading to the uniform modulated symbol vector $\mathbf{x}$. Theoretically, the BE scheme reinforces the decoding gain in the maximum *a posteriori* probability (MAP) decoder.

Then the standard OSDM modulation process can be expressed as [12]

$$s_{n',m} = \sqrt{N} \sum_{n=0}^{N-1} x_{n,m} e^{\frac{j2\pi nm}{N}}. \tag{1}$$

By stacking $\{s_{n',m}\}_{n'=0,m=0}^{N-1,M-1}$ rowwise, the precoded symbol vector is expressed as

$$\mathbf{s} = (\mathbf{F}_N^H \otimes \mathbf{I}_M)\mathbf{x} \tag{2}$$

where $\mathbf{s} = [s_0, s_1, \ldots, s_{K-1}]^T \in \mathcal{C}^{K \times 1}$ and $\mathbf{F}_N^H \otimes \mathbf{I}_M$ denotes interleaving operator involving N-point IFFT transformation and M-point Kronecker product. We assume $M > L$ to guarantee the equivalent channel matrix is valid, where L is the maximum channel length.

After cyclic prefix (CP) adding and removal at the both of the transceiver sides, the equivalent baseband received signal becomes

$$r_k = \sum_{l=0}^{L-1} h_{k,l} s_{k-1} + w_k, \ k = 0, \ldots, K-1 \tag{3}$$

where we assume the Doppler estimation and compensation is perfect or at least there is no significant effect on the channel equalization. During the block to be processed, the channel is assumed to be time-invariant and $\{h_l\}_{l=0}^{L-1}$ is the channel tap with L being the maximum channel length, w_k is the additive white Gaussian noise (AWGN) whose power is σ^2. The received signal vector is expressed as

$$\mathbf{r} = \tilde{\mathbf{H}}\mathbf{s} + \mathbf{w} \tag{4}$$

Here, we still adopt the previously defined single indexing with $\mathbf{r} = [r_0, r_1, \ldots, r_{K-1}]^T$ and $\tilde{\mathbf{H}}$ is the $K \times K$ circulant channel matrix with the first column equals to $[h_0, h_1, \ldots, h_{L-1}, 0, \ldots, 0]^T$. The OSDM demodulation process is the reversion of the modulation process, which needs the component-wise N-point FFT operator coupling with M-point Kronecker product. Analogous to (2), the OSDM demodulation process is expressed as

$$\mathbf{y} = (\mathbf{F}_N \otimes \mathbf{I}_M)\mathbf{r}. \tag{5}$$

where $\mathbf{y} = [\mathbf{y}_0^T, \mathbf{y}_1^T, \ldots, \mathbf{y}_{K-1}^T]^T$. Substituting (2) and (4) into (5), the I/O relationship of the OSDM system is written as

$$\mathbf{y} = \mathbf{H}\mathbf{x} + \mathbf{z} \tag{6}$$

where $\mathbf{z} = (\mathbf{F}_N \otimes \mathbf{I}_M)\mathbf{w}$ whose variance is σ_z^2, and

$$\mathbf{H} = (\mathbf{F}_N \otimes \mathbf{I}_M)\tilde{\mathbf{H}}(\mathbf{F}_N^H \otimes \mathbf{I}_M) \tag{7}$$

is the equivalent channel matrix that experiences the interleaving and de-interleaving procedures. Moreover, [12] has proved that if there is no time-varying nonlinear channel effects, the equivalent channel matrix is a block diagonal matrix $\mathbf{H} = \mathrm{Bdiag}\{\mathbf{H}_0, \mathbf{H}_1, \ldots, \mathbf{H}_{N-1}\}$ with the subblock matrix $\mathbf{H}_n$ being expressed as

$$\mathbf{H}_n = \boldsymbol{\Lambda}_M^{nH} \mathbf{F}_M^H \bar{\mathbf{H}}_n \mathbf{F}_n \boldsymbol{\Lambda}_M^n \tag{8}$$

with $\boldsymbol{\Lambda}_M^n = \mathrm{diag}\{[1, e^{-j2\pi n/K}, \ldots, e^{-j2\pi n(M-1)/K}]\}$, $\bar{\mathbf{H}}_n = \mathrm{diag}\{[H_n, H_{N+n}, \ldots, H_{(M-1)N+n}]\}$ and $H_k = \sum_{l=0}^{L-1} h_l e^{-j2\pi lk/K}, k = 0, \ldots, K-1$ being the channel response in frequency domain. The derivation of $\mathbf{H}_n$ in (8) is from the perspective of frequency domain, whereas, it can also be expressed in time domain as

$$\mathbf{H}_n = \begin{bmatrix} \tilde{h}_0 & 0 & \cdots & \bar{h}_{L-1} & \cdots & \bar{h}_1^{(n)} \\ \tilde{h}_1 & \tilde{h}_0 & 0 & \ddots & \ddots & \vdots \\ \vdots & \ddots & \ddots & \ddots & \ddots & \bar{h}_{L-1}^{(n)} \\ \tilde{h}_{L-1} & \ddots & \ddots & \tilde{h}_0 & \ddots & 0 \\ \vdots & \tilde{h}_{L-1} & \ddots & \ddots & \ddots & \vdots \\ 0 & \cdots & \tilde{h}_{L-1} & \cdots & \cdots & \tilde{h}_0 \end{bmatrix} \tag{9}$$

where $\tilde{h}_l = Nh_l$ and the inter-vector interference (IVI) components $\{\bar{h}_l^{(n)}\}_{l=1}^{L-1}$ at the upper right of (9) are expressed as

$$\bar{h}_l^{(n)} = \left(\sum_{n'=1}^{N-1} F_{n,n'} F_{n'-1,n}^* h_l \right) + F_{n,0} F_{N-1,n}^* h_l \tag{10}$$

with $F_{n,n'}$ and $F_{n',n}^*$ are the (n, n')th and (n', n)th entries of the FFT $\mathbf{F}$ and IFFT $\mathbf{F}^H$ matrices. Eq. (9) gives some basic insight of the OSDM scheme: 1) OSDM enjoys the diversity gain in frequency domain by collecting N times channel energy upon each subcarrier; 2) inter-vector interference (IVI) that obstructs the equalizer design must be considered.

After demodulation, the K-length signal block $\mathbf{y}$ in (6) are divided into N subvectors, i.e., $\mathbf{y}_n = [\mathbf{y}]_{nM:nM+M-1}$ and $\mathbf{z}_n = [\mathbf{z}]_{nM:nM+M-1}$ for $n = 0, 1, \ldots, N-1$, and thus the detection of the N signal subvectors in the OSDM can be decoupled in parallel as

$$\mathbf{y}_n = \mathbf{H}_n \mathbf{x}_n + \mathbf{z}_n, \ n = 0, 1, \ldots, N-1. \tag{11}$$

III. TIME DOMAIN SOFT-DECISION FEEDBACK EQUALIZER WITH SSIC

Now, we have the per vector system model in (11) as the candidate for channel equalization. However, we can't use $\mathbf{H}_n$ to design the equalizer directly because of the asymmetric post-cursor IVI from $\bar{h}_l^n$ which needs to be removed at current symbol vector $\mathbf{x}_n$. Specifically, when the nth subvector is equalized in the previous iteration, the soft-decision $\breve{x}_{n,m}$ are

then available for the post-cursor IVI reconstruction and then removed as

$$\hat{\mathcal{I}}_{n,m} = \sum_{l=m+1}^{L-1} \bar{h}_l^{(n)} \breve{x}_{n,M-l+m} \quad (12a)$$

$$y'_{n,m} := y_{n,m} - \hat{\mathcal{I}}_{n,m} \quad (12b)$$

for $0 \leq m \leq L - 2$. After the post-cursor effect is removed, the refined received signal block is re-arranged as

$$\mathbf{y}_n \triangleq [y'_{n,0}, \ldots, y'_{n,L-2}, y_{n,L-1}, \ldots, y_{n,M-1}]^T \quad (13)$$

and $\mathbf{H}_n$ becomes a normal zero forcing Toeplitz matrix with $\bar{h}_l^{(n)}$ being removed. Now, we can design the per vector equalizer under decision feedback mode, leading to the nth subvector output as

$$\hat{\mathbf{x}}_{n,m} = \mathbf{W}_n \left(\mathbf{y}_n - \hat{\mathbf{H}}_n \bar{\mathbf{x}}_{n,m} \right) - \mathbf{B}_n \left(\breve{\mathbf{x}}_{n,m} - \bar{\mathbf{x}}_{n,m} \right) + \bar{\mathbf{x}}_{n,m} \quad (14)$$

where $\mathbf{W}_n \in \mathcal{C}^{M \times M}$ and $\mathbf{B} \in \mathcal{C}^{M \times M}$ are the feedforward and feedback equalizer matrices, respectively. In order to perform SSIC, the feedback matrix $\mathbf{B}_n$ is designed as a zero-diagonal upper triangular matrix. The vector $\bar{\mathbf{x}}_{n,m}$ is obtained by setting the mth entry of the *a priori* mean subvector $\bar{\mathbf{x}}_n \triangleq \mathbf{E}[\mathbf{x}_n] = [\bar{x}_{n,0}, \ldots, \bar{x}_{n,M-1}]^T \in \mathcal{C}^{M \times 1}$ as zero while keeping all the other entries unchanged, expressed as $\bar{\mathbf{x}}_{n,m} = [\bar{x}_{n,0}, \ldots, \bar{x}_{n,m-1}, 0, \bar{x}_{n,m+1}, \ldots, \bar{x}_{n,M-1}]^T$. The self-subtraction avoids the instability caused by the positive feedback during the iteration operation, i.e., the *a priori* information of $x_{n,m}$ should not be used during the detection of $x_{n,m}$ itself.

The vector $\breve{\mathbf{x}}_n = [\breve{x}_{n,0}, \ldots, \breve{x}_{n,M-1}]^T \in \mathcal{C}^{M \times 1}$ contains the *a posteriori* means obtained from the previous and current turbo iteration. If the error-free feedback is assumed, i.e., $\breve{\mathbf{x}}_n = \mathbf{x}_n$, the equalizer matrices $\mathbf{W}_n$ and $\mathbf{B}_n$ are calculated by minimum mean square error (MMSE) criteria as

$$\mathbf{W}_n = \mathbf{U}_n \mathbf{\Phi}_n \mathbf{H}_n^H \left[\mathbf{H}_n \mathbf{\Phi}_n \mathbf{H}_n^H + \sigma_z^2 \mathbf{I}_M \right]^{-1} \quad (15a)$$

$$\mathbf{B}_n = \mathbf{U}_n - \mathbf{I}_M \quad (15b)$$

where the ideal channel matrix $\mathbf{H}_n$ is used to replace the estimated $\hat{\mathbf{H}}_n$. The diagonal matrix $\mathbf{\Phi}_n \triangleq \mathbf{E}[(\hat{\mathbf{x}}_n - \bar{\mathbf{x}}_n)(\hat{\mathbf{x}}_n - \bar{\mathbf{x}}_n)^H]$ is the covariance matrix of $\mathbf{x}_n$, simplified as

$$\mathbf{\Phi}_n = \mathrm{diag}[\sigma_{x_{n,0}}^2, \ldots, \sigma_{x_{n,m-1}}^2, 1, \sigma_{x_{n,m+1}}^2, \ldots, \sigma_{x_{n,M-1}}^2] \quad (16)$$

in which definition, the mean and variance of $x_{n,m}$ to be detected, are assumed to be 0 and 1, respectively. The upper triangular matrix $\mathbf{U}_n$ is obtained by performing the Cholesky decomposition as

$$\mathbf{U}_n^H \mathbf{\Delta}_n \mathbf{U}_n = \mathbf{\Phi}_n^{-1} + \frac{1}{\sigma_z^2} \mathbf{H}_n^H \mathbf{H}_n \quad (17)$$

Furthermore, the system model in (14) is represented alternately as

$$\tilde{\mathbf{r}}_n \triangleq \mathbf{W}_n \left(\mathbf{y}_n - \mathbf{H}_n \bar{\mathbf{x}}_{n,m} \right) = \mathbf{U}_n \left(\hat{\mathbf{x}}_n - \bar{\mathbf{x}}_{n,m} \right) + \mathbf{e}_{n,m} \quad (18)$$

where $\tilde{\mathbf{r}}_n = [\tilde{r}_{n,0}, \tilde{r}_{0,1}, \ldots, \tilde{r}_{n,M-1}]$ conveys the residual samples of the corresponding subvectors and $\mathbf{e}_{n,m} = \tilde{\mathbf{x}}_{n,m} - \mathbf{x}_n$

is the residual decision error. Once $\tilde{\mathbf{r}}_n$ is acquired, we can calculate the *a posteriori* probability of $\breve{x}_{n,m}$ at current turbo iteration as

$$\breve{x}_{n,m} = \sum_{\alpha_i \in \mathcal{S}} \alpha_i \mathrm{Pr}(x_{n,m}^{(i)} = \alpha_i | \tilde{\mathbf{r}}_n) \quad (19)$$

which is used for (14). For the extrinsic information iteration between the equalizer and MAP decoder, and the BCJR algorithm itself is out of the scope in this paper and will not be detailed.

IV. SIMULATION

We compared the proposed per vector SDFE with the conventional block-wise MMSE equalizer where the equalized symbol vector is expressed as

$$\mathbf{y} = (\mathbf{H}^H \mathbf{H} + \sigma_z^2 \mathbf{I})^{-1} \mathbf{H}^H \mathbf{x}. \quad (20)$$

The testbench adopted the direct playback simulator [14] under the UWA channels truncated from the field experiment. Figure 1 demonstrates the channel evolution used in this simulation. The channel energy was majorly distributed with the first 60 channel taps, and we fixed the maximum channel length as $L = 100$. The length of $\mathbf{x}$ used in this simulation was chosen as $K = 1024$ with QPSK modulation both in BE and VE schemes. We set parameters $N = 4$ and $M = 256$.
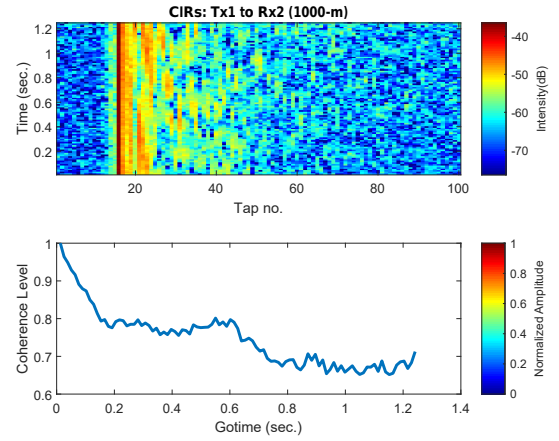

Fig. 1. CIR evolution and the corresponding coherence time used for simulation.

Figure. 2 illustrates the BER performance with BE and VE schemes under SDFE, where the BE scheme outperformed the VE scheme by 0.5 dB when the BER was on the order of 10^{-4} at the second turbo iteration. The BER curves also demonstrate that the encoding gain of BE scheme over VE scheme was insignificant at low SNR, but will increase when the SNR becomes higher.

Figure. 3 gives the BER comparison of the OSDM with SDFE and MMSE equalizers. We increased $N = 8$ and kept $M = 256$ unchanged. However, the BER performance of BE-SDFE seemed to have no significant improvement compared to Fig. 2, which was attributed to the excessive block
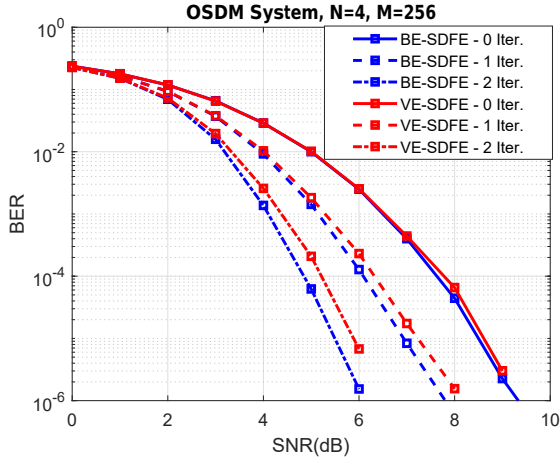
Fig. 2. Simulated BER performance of OSDM with BE and VE schemes with the proposed SDFE-TEQ.
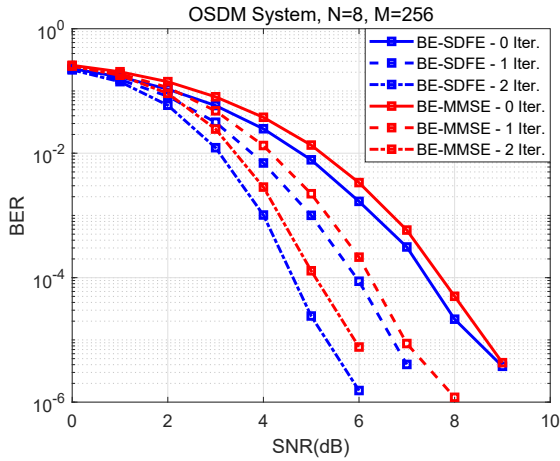

Fig. 3. Simulated BER performance of OSDM with SDFE and MMSE TEQ.

length compared with the channel coherence time. The system degradation also gives the philosophy of the system design that the time invariant assumption of UWA channels should consider the channel dynamics at least the channel coherence time. Nevertheless, the SDFE still had better performance than the MMSE proving that the proposed SDFE structure is valid in the OSDM receiver design.

V. Experimental Results

The experiment was conducted in March, 2019, the area of Zhairuoshan Island, East China Sea, at a sea depth about 20 m. The communication distance was about 800 m with one transducer and three hydrophones. The carrier frequency was 12 kHz with a 7.812 kHz bandwidth. The signal frame is depicted in Fig. 4, where each OSDM block contained ten OSDM subblocks ahead padding with m-sequence and guard intervals which are not drawn in the above figure, each subblock carriers 1024 payload symbols encoded with $[17, 13]_{oct}$ convolutional code with BE or VE schemes. The LFM signals were served to synchronize the signal, measure the channel length, and estimate the primary Doppler shift. We also utilized the m-sequence to estimate the channel and performed the refined Doppler shift tuning.

LFM	GAP	M-seq	BE-OSDM QPSK	GAP	M-seq	BE-OSDM 8PSK	GAP	M-seq	BE-OSDM 16QAM	LFM

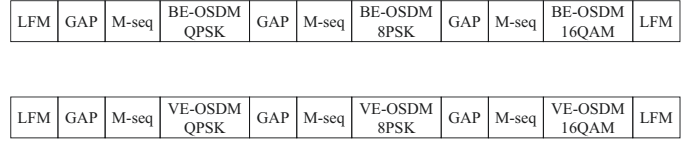| LFM	GAP	M-seq	VE-OSDM QPSK	GAP	M-seq	VE-OSDM 8PSK	GAP	M-seq	VE-OSDM 16QAM	LFM

Fig. 4. Transmitted signal frame with BE and VE encoding schemes.

Five recorded epoch files (from epoch 1 to epoch 5) with $N = 4$ and $M = 256$ were processed in this paper. Table I illustrates the BER comparison between the BE-SDFE and VE-SDFE with different modulation size (QPSK, 8PSK, 16QAM), where the testbench adopted one hydrophone without array diversity gain. Epoch 1 and Epoch 3 had the best and worst BER performance among the five processed data files. Figure 5 demonstrates the channel conditions of epoch 1 and epoch 3. Obviously, data in Epoch 3 suffered much more severe channel selectivity that had a Doppler scale with 20 Hz spread and 5 Hz shift. Also, the received signal power was much lower due to more reflections and distortions. Moreover, the BE-SDFE outperformed the VE-SDFE thanks to the decoding gain from the MAP decoder.

VI. Conclusion

This paper proposes a time domain per vector SDFE for OSDM UWA communications. With the refined Doppler post-processing and IVI elimination, the equivalent channel matrix enhances the SDFE via SSIC. Simulation results show that the SDFE outperforms the conventional block-wise MMSE and the BE scheme has more encoding and decoding gains than the VE scheme. Similar result is also drawn from the experimental data processing. Also, there still some improvement remained for the proposed approaches such as the decoding gain of the BE over the VE is insignificant, and the equivalent channel matrix depends on the residual Doppler that the system model should incorporate with the resilient Doppler effect. All of these shall be suspended for the future work.

VII. Acknowledgement

TABLE I
BER COMPARISON OF THE OSDM WITH BE-SDFE AND VE-SDFE

Epoch No.	QPSK		8PSK		16QAM	
	BE-SDFE	VE-SDFE	BE-SDFE	VE-SDFE	BE-SDFE	VE-SDFE
1	2.16×10^{-4}	4.58×10^{-4}	8.57×10^{-4}	9.68×10^{-4}	4.07×10^{-3}	4.94×10^{-3}
2	7.05×10^{-4}	9.53×10^{-4}	1.03×10^{-3}	1.71×10^{-3}	3.52×10^{-2}	3.79×10^{-2}
3	4.74×10^{-3}	5.21×10^{-3}	8.52×10^{-3}	9.35×10^{-3}	6.91×10^{-2}	7.47×10^{-2}
4	8.46×10^{-4}	9.64×10^{-4}	1.24×10^{-3}	2.02×10^{-3}	3.76×10^{-2}	3.93×10^{-2}
5	2.31×10^{-3}	2.83×10^{-3}	4.59×10^{-3}	6.07×10^{-3}	4.26×10^{-2}	4.51×10^{-2}

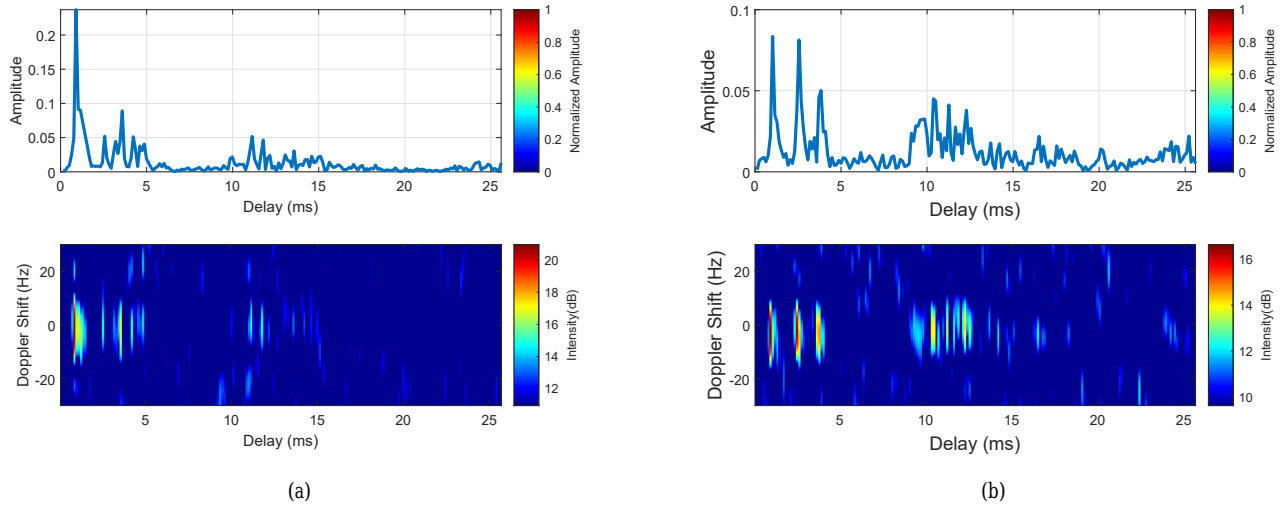(a)   (b)

Fig. 5.   The estimated CIRs and the corresponding scattering function corresponding to Epoch 1 and Epoch 3.

REFERENCES

[1] Y. R. Zheng, J.Wu, and C. Xiao, "Turbo equalization for single-carrier underwater acoustic communications," *IEEE Commun. Mag.*, vol. 53, no. 11, pp. 79–87, Nov. 2015.

[2] F. Qu, Z. Wang, and L. Yang", "Differentially orthogonal space-time block coding modulation for time-variant underwater acoustic channels," *IEEE J. Oecan. Eng.*, vol. 42, no. 1, pp. 188–198, Jan. 2017.

[3] B. Li and J. Huang and S. Zhou and Keenan Ball and M. Stojanovic and L. Freitag and P. Willett, "MIMO-OFDM for high-rate underwater acoustic communication," *IEEE J. Oecan. Eng.*, vol. 34, no. 4, pp. 634–644, Oct. 2009.

[4] C. R. Berger and S. Zhou, "Sparse channel estimation for multicarrier underwater acoustic communication: from subspace methods to compressed sensing," *IEEE J. Oecan. Eng.*, vol. 58, no. 3, pp. 1708–1721, Mar. 2010.

[5] B. F. Boroujeny, "OFDM versus filter bank multicarrier," *IEEE Singal Process. Mag.*, vol. 28, no. 3, pp. 92–112, May 2011.

[6] N. Nichailow, M. Matth, I. S. Gaspar, A. N. Caldevilla, L. L. Mendes, A. Festag, and G. Fettweis, "Generalized frequency division multiplexing for 5th generation cellular networks," *IEEE Trans. Commun.*, vol. 62, no. 9, pp. 3045–3061, Sept. 2014.

[7] L. Dai, B. Wang, Y. Yuan, S. Han, C. I, and Z. Wang, "Non-orthogonal multiple access for 5G: solutions, challenges, opportunities, and future research trends," *IEEE Commun. Mag.*, vol. 53, no. 9, pp. 74–81, Sept. 2015.

[8] X. G. Xia, "Precoded and vector OFDM robust to channel spectral nulls and with reduced cyclic prefix length in single transmit antenna systems," *IEEE Trans. Commun.*, vol. 49, no. 8, pp. 1363–1374, Aug. 2001.

[9] N. Suehiro, C. Han, T. Imoto, and N. Kuroyanagi, "An information transmission method using Kronecker product", in *Proc. IASTED Int. Conf. Commun. Systems Networks*, pp. 206-209, Sept. 2002.

[10] T. Ebihara and K. Mizutani, "Underwater acoustic communication with an orthogonal signal division multiplexing scheme in doubly spread channels," *IEEE J. Ocean. Eng.*, vol. 39, no. 1, pp. 4758, Jan. 2014.

[11] T. Ebihara and G. Leus, "Doppler-resilient orthogonal signal-division multiplexing for underwater acoustic communication," *IEEE J. Ocean. Eng.*, vol. 41, no. 2, pp. 408427, Apr. 2016.

[12] J. Han, S. P. Chepuri, Q. Zhang, and G. Leus, "Iterative per-vector equalization for orthogonal signal-division multiplexing over time-varying underwater acoustic channels," *IEEE J. Ocean. Eng.*, vol. 44, no. 1, pp. 240–255, Jan. 2019.

[13] J. Han, Y. Wang, L. Zhang, and G. Leus, "Time-domain oversampled orthogonal signal-division multiplexing underwater acoustic communications," *J. Acoust. Soc. Am.*, vol. 145, no. 1, pp. 292–300, Jan. 2019.

[14] R. Otnes, P. A. van Walree, and T. Jenserud, "Validation of replay-based underwater acoustic communication channel simulation", *IEEE J. Ocean. Eng.*, vol. 38, no. 4, pp. 689–700, 2013.